Advances in imaging instrumentation for nuclear cardiology

Jae Sung Lee, PhD,[a,b] Gil Kovalski, PhD,[c] Tali Sharir, MD,[d,e] and Dong Soo Lee, MD, PhD[a,f]

[a] Department of Nuclear Medicine, Seoul National University College of Medicine, Seoul, Korea
[b] Department of Biomedical Sciences, Seoul National University College of Medicine, Seoul, Korea
[c] General Electric Healthcare, Haifa, Israel
[d] Department of Nuclear Cardiology, Assuta Medical Centers, Tel Aviv, Israel
[e] Faculty of Health Sciences, Ben-Gurion University of the Negev, Beer-Sheva, Israel
[f] Department of Molecular Medicine and Biopharmaceutical Sciences, Graduate School of Convergence Science and Technology, Seoul National University, Suwon, Korea

Received Mar 5, 2017; accepted Jun 8, 2017
doi:10.1007/s12350-017-0979-8

Advances in imaging instrumentation and technology have greatly contributed to nuclear cardiology. Dedicated cardiac SPECT cameras incorporating novel, highly efficient detector, collimator, and system designs have emerged with the expansion of nuclear cardiology. Solid-state radiation detectors incorporating cadmium zinc telluride, which directly convert radiation to electrical signals and yield improved energy resolution and spatial resolution and enhanced count sensitivity geometries, are increasingly gaining favor as the detector of choice for application in dedicated cardiac SPECT systems. Additionally, hybrid imaging systems in which SPECT and PET are combined with X-ray CT are currently widely used, with PET/MRI hybrid systems having also been recently introduced. The improved quantitative SPECT/CT has the potential to measure the absolute quantification of myocardial blood flow and flow reserve. Rapid development of silicon photomultipliers leads to enhancement in PET image quality and count rates. In addition, the reduction of emission–transmission mismatch artifacts via application of accurate time-of-flight information, and cardiac motion de-blurring aided by anatomical images, are emerging techniques for further improvement of cardiac PET. This article reviews recent advances such as these in nuclear cardiology imaging instrumentation and technology, and the corresponding diagnostic benefits. (J Nucl Cardiol 2019;26:543–56.)

Key Words: SPECT • SPECT/CT • PET • PET/CT • PET/MRI

Abbreviations

MPI	Myocardial perfusion imaging
CAD	Coronary artery disease
PMT	Photomultiplier tube
CZT	Cadmium zinc telluride
CAC	Coronary artery calcium
MBF	Myocardial blood flow
MFR	Myocardial flow reserve
TOF	Time-of-flight
APD	Avalanche photodiode
SiPM	Silicon photomultiplier

Electronic supplementary material The online version of this article (doi:10.1007/s12350-017-0979-8) contains supplementary material, which is available to authorized users.

The authors of this article have provided a PowerPoint file, available for download at SpringerLink, which summarizes the contents of the paper and is free for re-use at meetings and presentations. Search for the article DOI on SpringerLink.com.

Reprint requests: Dong Soo Lee, MD, PhD, Department of Nuclear Medicine, Seoul National University College of Medicine, 103 Daehak-ro, Jongno-gu, Seoul 110-799, Korea; *dsl@plaza.snu.ac.kr*; Tali Sharir, MD, Department of Nuclear Cardiology, Assuta Medical Centers, 96 Igal Alon, C Building, 67891 Tel Aviv, Israel; *tsharir@gmail.com*

1071-3581/$34.00

See related editorial, pp. 557–560

INTRODUCTION

The two principal imaging modalities used in nuclear cardiology are single photon emission computed tomography (SPECT) and positron emission tomography (PET). Hybrid imaging systems in which SPECT and PET are combined with computed tomography (CT) are also widely used, and hybrid magnetic resonance imaging (MRI) and PET systems have recently been introduced. The field of nuclear cardiology has benefited from the development of these devices and numerous radiotracers for imaging.

Myocardial perfusion imaging (MPI) with electrocardiogram (ECG)-gated SPECT is a useful imaging tool for the detection of coronary artery disease (CAD) and determination of prognosis. However, conventional SPECT cameras comprise sodium iodide (NaI) detectors and large photomultiplier tubes (PMTs) that yield suboptimal photon detection and processing, and hence compromised image quality images. Dedicated cardiac SPECT cameras incorporating more efficient detector, collimator, and system designs have emerged with the expansion of nuclear cardiology.[1–3] The new cameras yield high-resolution images acquired over considerably short time periods, with reduced patient radiation exposure and improved diagnostic accuracy. Solid-state radiation detectors comprising cadmium zinc telluride (CZT), which directly convert radiation to electrical signals and yield enhanced count sensitivity (when combined with a customized collimator), energy resolution, and spatial resolution as compared with other currently available detectors, are increasingly gaining favor as the detector of choice. Some of these cardiac SPECT scanners allow the stationary data acquisition with no camera rotation for dynamic SPECT scanning.

Another recent advance is the hybrid SPECT/CT system. Using reliable attenuation and scatter corrections of perfusion images, as compared with SPECT imaging alone, these hybrid systems improve the diagnostic accuracy and reduce the rate of artifacts that commonly confound the interpretation of myocardial SPECT scans. Moreover, several of these systems allow low-dose coronary artery calcium (CAC) scoring assessment in conjunction with MPI, thereby providing additional anatomic and prognostic information, which is valuable among patients with no history of coronary artery disease.[4]

In comparison with SPECT, cardiac PET possesses superior diagnostic accuracy with regard to coronary artery disease detection because PET typically yields higher spatial resolution and better contrast-to-background ratio. In addition, the ring-shaped arrangement of PET detectors and electronic collimation using coincidence logic affords dynamic PET scans with high-count sensitivity that enables routine quantification of absolute myocardial blood flow (MBF) and myocardial flow reserve (MFR). Hybrid PET/CT systems equipped with a high-end multi-detector CT scanner are currently widely used, allowing for the comprehensive combined anatomical and functional evaluation of coronary diseases. In recent years, combined PET/MRI systems have emerged with new perspectives in cardiac imaging beyond the scope of MPI.[5,6] PET detectors employing solid-state photosensors and advanced scintillators are rapidly evolving and warrant the higher PET system performance in future PET/CT and PET/MRI systems.[7,8]

The aim of this article is to review recent technological advances in imaging instrumentations employed in nuclear cardiology. However, its scope is limited to the most recent innovations applied to current clinical imaging systems. Although many of the technologies mentioned in this article are not limited to cardiac imaging, we emphasize the efforts made to improve diagnostic performance for the detection of heart disease.

SPECT AND SPECT/CT

The efficacy and quality of SPECT scans are fundamentally dependent on properties of the collimator and detection media, in addition to the reconstruction technique. Over the last few decades, various design alternatives have been applied to increase system efficiency in detecting emitted photons while maintaining adequate image resolution.

Reconstruction Algorithms

The advancements in computer power, in addition to increased availability of SPECT/CT systems, have led to wide adaptation of iterative reconstruction algorithms in SPECT. These algorithms were further improved to model physical properties such as attenuation correction and collimator response and require shorter acquisition time or reduced injected dosage. A detailed comparison of the performance of various algorithms provided by manufacturers has been reviewed by Knoll et al.[9] Borges-Neto et al.[10] evaluated the wide beam reconstruction method (WBR^{TM} developed by UltraSPECT Inc.) for decreasing scan times as compared with filtered back projection (FBP). These investigators demonstrated that using WBR with half the scan time of FBP reconstruction did not compromise the qualitative or quantitative measurements. Ali et al.[11] have demonstrated that the quantitative measurements of Evolution for Cardiac (trademark of General Electrical Company) using half-time acquisition provided clinical diagnosis in concordance with that from

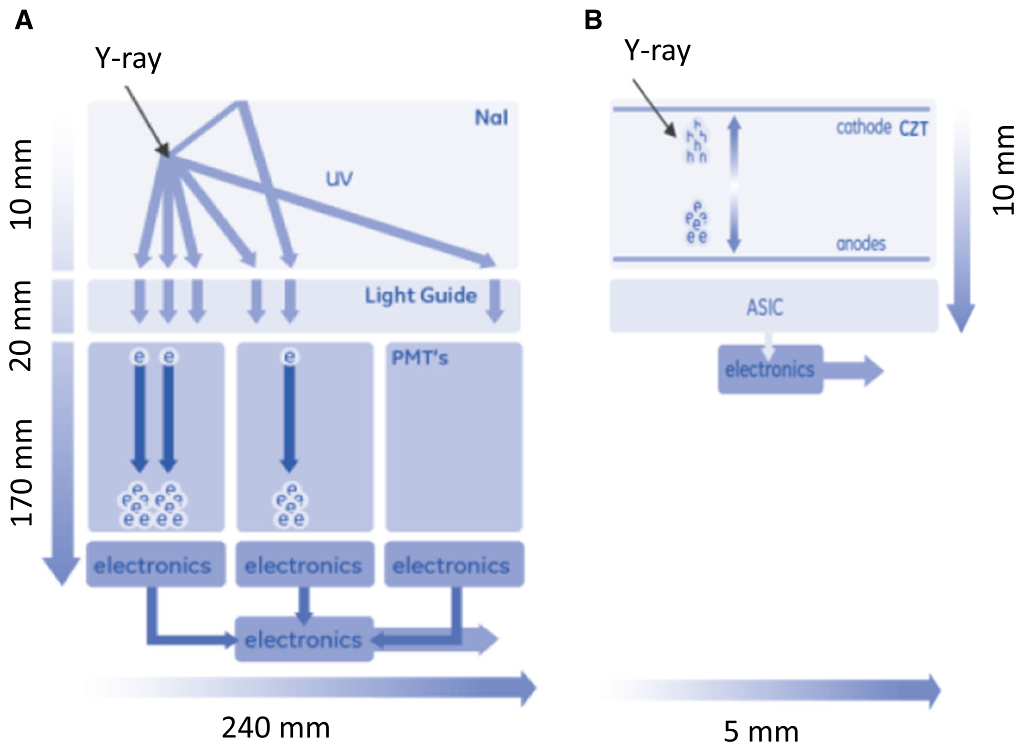

Figure 1. A Indirect conversion of gamma-photon energy into an electrical signal using NaI crystal coupled with PMTs, versus direct conversion using CZT detectors (**B**).

full-time acquisition for both attenuation-corrected and non-corrected reconstructions.

Dedicated Cardiac CZT Scanners

Improvement in cardiac SPECT system efficiency has accompanied the introduction of CZT pixelated solid-state detectors over the last ten years. Acquisition times of systems employing CZT detectors exhibited approximately five-fold reductions, yielding acquisition times as short as 2-3 min per scan.[1–3,12] The fundamental difference between NaI detectors employed by conventional systems and CZT detectors is the conversion process of the photon energy into an electrical signal. In NaI-based detection, this energy conversion is carried out indirectly via a scintillation process. Conversely, CZT conversion does not employ the method of scintillation, as gamma-photon energy is directly converted into an electrical signal at the CZT module level through solid-state technology (Figure 1).

The principal practical advantages of utilizing CZT detectors are as follows: (1) it possesses a pixelated nature improving the intrinsic resolution that affords higher system resolution; and (2) it offers a substantially reduced physical size as compared with NaI-PMT-based detectors, thereby leading to compact efficient designs and energy resolution enhancements, which consequently yield an improved photon detection mechanism. The pixelated detector reduces the uncertainty originating from the intrinsic resolution of a gamma detector. In a pixelated CZT detector, each 2.56 mm pixel is supported by its own electronic circuit, thus the uncertainty regarding the point of interaction is bounded by the size of the pixel. The small physical size of the CZT module affords efficient system designs with small footprint and in-focus detection of the heart. Therefore, at any given point in time, the detectors are primarily detecting photons originating from and near the heart, and not from the entire body.

The improvement in energy resolution yields two major benefits. First, it has the capacity to permit narrowing of the energy window typically used for NaI detectors. Secondly, it enables simultaneous acquisition of photons emitted from multiple isotopes with similar energy levels. The energy window used for ^{99m}Tc-based radiopharmaceuticals is commonly set to 20% of the 140.5 keV photo-peak to account for the limited energy resolution of the NaI detector. As such, scattered photons, which have been re-directed due to photon-tissue interaction, having energy within this window range are detected as true counts. The enhanced energy resolution of the CZT detector (6.3%-9.5%) allows using a narrowed window and reduction in the number

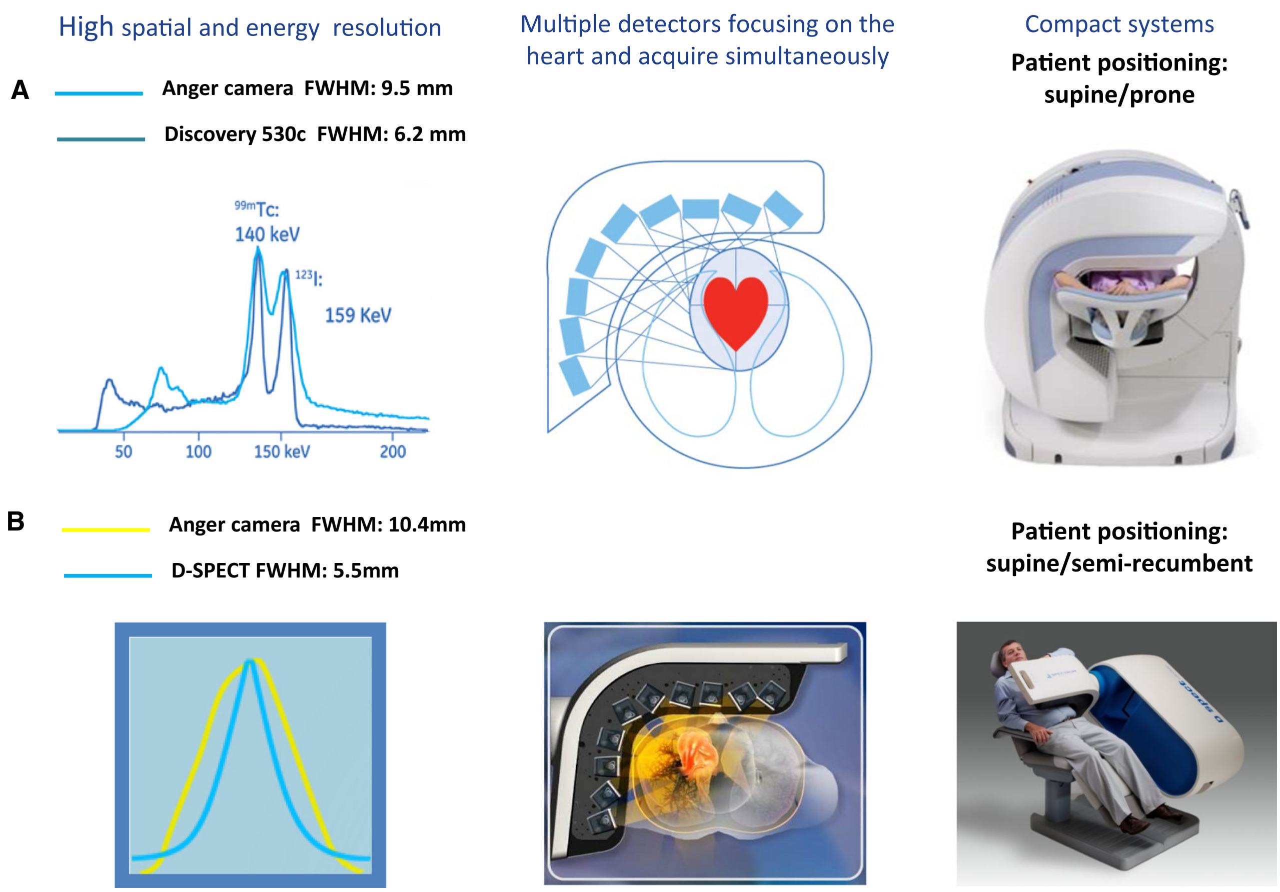

Figure 2. Two different CZT cameras: **A** discovery NM 530c, and **B** D-SPECT that use multiple CZT detectors focusing on the heart and acquire data simultaneously, providing high spatial and energy resolution (image courtesy of GE Healthcare and Biosensors).

of scattered photons entering the main photo-peak window. The reduced crosstalk in dual-isotope simultaneous acquisition is another benefit of the enhanced energy resolution of CZT detector. Dual-isotope acquisition may play an important role with the clinical benefit of innervation imaging using ^{123}I-based agents in the presence of ^{99m}Tc perfusion agents.

At present, hundreds of dedicated cardiac systems are used worldwide. The two most common CZT-based cardiac systems are the Discovery NM 530c™ (D530c) manufactured by General Electrical, and D-SPECT™ manufactured by Biosensors™ (Figure 2). However, there is a distinct difference in their system designs. While the D530c employs a stationary pinhole-based collimator,[13] the D-SPECT uses a high-sensitivity parallel hole swinging collimator.[1] Both systems effectively exploit the small size of the CZT module to efficiently detect photons originating near the heart. The D530c uses a three-dimensional maximum likelihood reconstruction, while the D-SPECT employs a cardiac prior to further boost image quality. A detailed performance comparison between the two systems has been summarized by Imbert et al.[14] and Zoccarato et al.[15]

To date, multiple studies have reviewed the clinical efficacy of these systems. Sharir et al.[1] have described their initial experiences using the high-speed D-SPECT system in comparison with the conventional NaI system. This particular publication was followed by multicenter studies reported by Esteves et al.[2] and Sharir et al.[3] using the D530c and D-SPECT systems, respectively; results of these studies yielded similar performance of the CZT-based cameras and conventional cameras at markedly reduced acquisition times of five- to seven-fold. Duvall et al.[16] demonstrated the diagnostic value of the D530c camera using invasive coronary angiography as the gold standard.

The enhancements in system performance have led investigators to further explore methods to achieve the reduction of injected dosage. Einstein et al.[17] have demonstrated the following results: (1) the radiation dose can be reduced to a range of 1-2 mSv using the CZT-based system, and (2) its image finding was highly

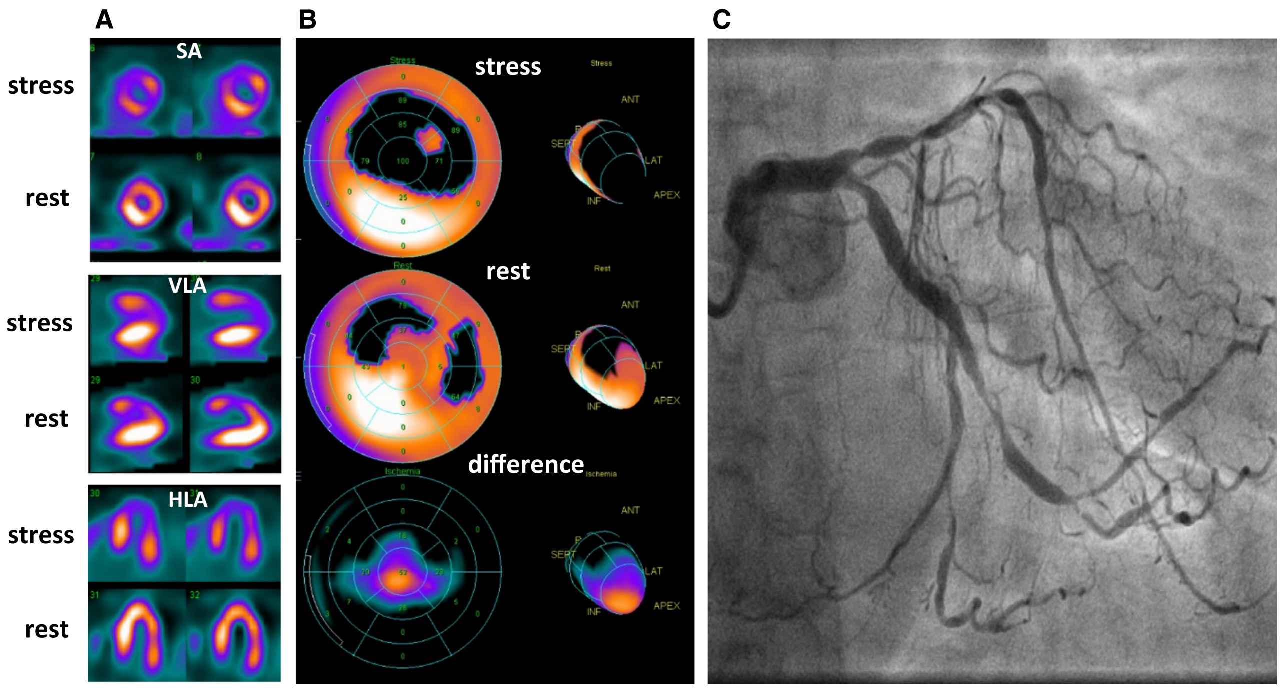

Figure 3. **A** Perfusion images and **B** quantitative polar maps obtained from an obese female undergoing low-dose TC-99m sestamibi CZT-MPI, showing excellent image quality and high correlation to the invasive coronary angiography (C).

correlated to standard low dose scans. Upon utilizing invasive coronary angiography as the gold standard, Sharir et al.[18] have shown that the diagnostic performance of half-dose stress-first fast SPECT is comparable to that of standard-dose MPI with regard to identification of significant coronary disease. Using ultra-low stress-dose under 2 mSv, the quantitative stress-perfusion deficit yielded excellent diagnostic performance, with area under the receiver operator characteristic curve of 91.5% for the supine, and 93.5% for prone imaging; these results were superior to previously published data for full-dose, conventional SPECT imaging. Figure 3 shows low-dose 6 mCi stress / 18 mCi rest Tc-99m sestamibi images obtained from a 64-year-old diabetic female with BMI = 35 kg/m^2 using the discovery 530c CZT camera. Perfusion images demonstrated severe ischemia in the left anterior descending (LAD) coronary artery territory, and mild ischemia in the left circumflex/marginal distribution (Figure 3A). Quantitative analysis using quantitative perfusion SPECT (QPS, CSMC, Los Angeles, CA) and custom normal limits, specific to the discovery 530c camera[18] demonstrated extensive ischemia (Figure 3B) that highly correlated to the results of invasive coronary angiography (Figure 3C).

Absolute quantitation and blood flow measurements may lead to the improved diagnostic accuracy of MPI via increased detection of balanced ischemia and multivessel disease. Ben-Haim et al.[19] have demonstrated that the retention indices describing perfusion reserve are lower in patients with perfusion defects and in regions supplied by obstructed coronary arteries. Boullegue et al.[20] have shown in a pilot study that the myocardial perfusion reserve correlated well with corresponding angiographic findings and fractional flow reserve measurements. Although these studies have demonstrated the feasibility of perfusion reserve measurements, absolute flow measurements are also just in the pipeline.[21]

SPECT/CT Systems

Along with the wide adoption of SPECT/CT systems, attenuation correction and CAC deposit assessment can be used to further improve reading confidence and boost stress-only protocol adaptation. Mouden et al.[22] investigated the influence of the CAC score on the interpretation of MPI. This study concluded that knowledge of the CAC score increased certainty and reduced equivocal interpretations. Figure 4 demonstrates a SPECT/ CT study (Discovery 670, GE Heathcare, Israel) of a 72-year-old male with history of hypertension and dyslipidemia, presenting with atypical chest pain and a non-diagnostic stress ECG.

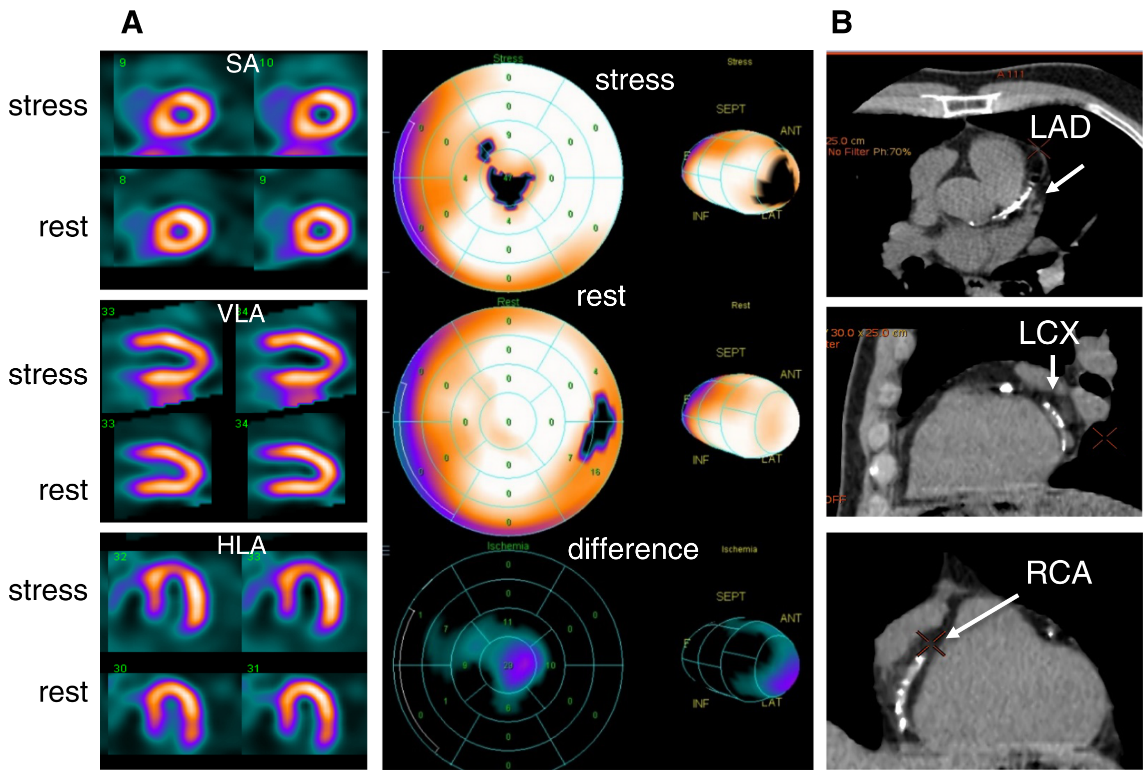

Figure 4. SPECT-MPI and CT-CAC of a 72-year-old male obtained via a SPECT/CT camera. **A** MPI showing only mild ischemia, and **B** CT demonstrating extensive coronary artery calcification.

Dipyridamole stress/rest Tc-99m sestamibi MPI combined with CAC assessment demonstrated only mild infero-apical ischemia, but showed extensive coronary artery calcification of the three coronary arteries (CAC score = 1, 384). Invasive coronary angiography demonstrated extensive coronary artery disease with proximal and distal involvement of the three coronary arteries and branches, and a mild left main lesion. The patient underwent coronary artery bypass grafting.

Chang et al.[23] have studied the relationship between CAC score and MPI-SPECT for predicting short- and long-term risk of cardiac events. They concluded that these tests were independent and complementary. Further development of hybrid SPECT/CT systems to enable low-dose SPECT-MPI combined with coronary angiography will provide a comprehensive assessment of myocardial perfusion, coronary calcification, and coronary anatomy.

While the potential of MPI-SPECT is yet to be fully realized, recent technologies have provided the clinicians with solid tools to advance the efficacy of the modality by reducing dosage, increasing accuracy, and reducing cost.

Quantitative SPECT/CT

SPECT is commonly regarded as less accurate than PET in terms of absolute quantification of radioactivity concentration. Still the majority of cardiac SPECT studies are performed without correction for attenuation, the main source of quantitative error in emission tomography. External radionuclide sources have not been widely used for attenuation and scatter corrections because the transmission scans using those may produce additional artifacts associated with low counting statistics and body truncation in attenuation maps. Alternatively, the combined SPECT/CT provides more reliable attenuation maps with high counting statistics, thus enhancing quantitative SPECT imaging. The quantitative accuracy of ^{99m}Tc SPECT images corrected for attenuation and scatter via incorporation of CT information in the SPECT reconstruction is equivalent to that of PET images in terms of standard uptake values (SUV).[24]

The quantitatively enhanced SPECT/CT enables the absolute quantification of MBF and MFR, useful variables for identifying multivessel CAD and predicting the extent of CAD with greater accuracy than methods of relative quantification or visual analysis of MPI.[25,26] In a recent dynamic SPECT measurement study using GE D530c, the MBF values measured using quantitative ^{201}TI, ^{99m}Tc-tetrofosmin, and ^{99m}Tc-sestamibi SPECT scans corrected using separately acquired CT data were found to correlate well with microsphere MBF in a

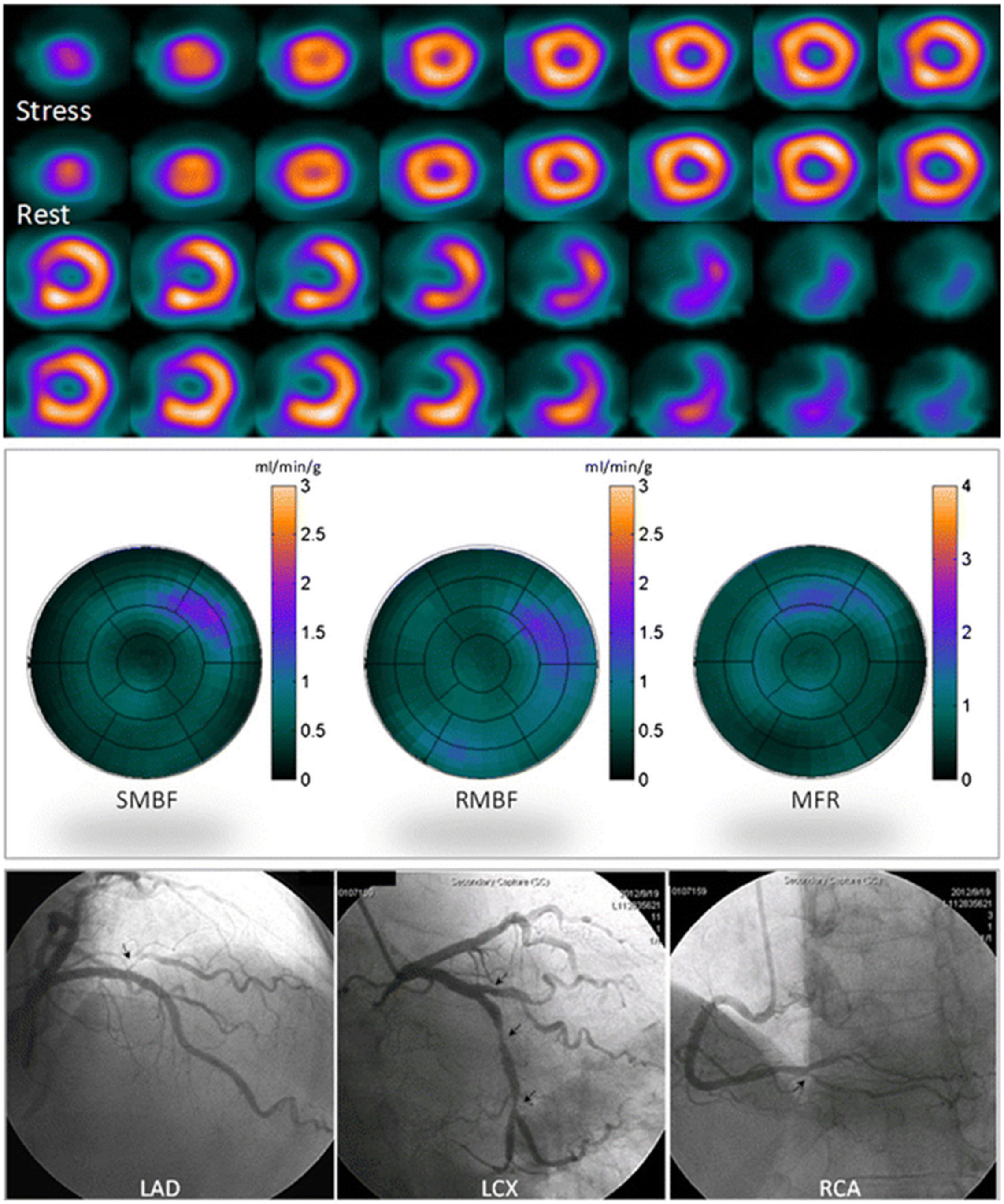

Figure 5. Image taken from a 71-year-old male patient demonstrating enhanced CAD detection power acquired via quantitative dynamic SPECT scan in three-vessel CAD. The coronary angiography confirmed severe stenosis in the 1st diagonal, left circumflex, and right posterior descending arteries. (Reprint from Ref. Hsu et al.[30] with permission).

porcine CAD model.[27] The absolute MBF measurements were also obtained using a conventional, slowly rotating dual-head SPECT camera in a SPECT/CT (Philips Precedence 16).[28] In this study, a spatiotemporal iterative reconstruction method providing the coefficients of a set of continuous basis functions per voxel was used to overcome problems associated with the low temporal sampling rate of conventional SPECT. Moreover, the enhanced temporal resolution of modern SPECT/CT systems allows absolute MBF quantification using a standard iterative SPECT reconstruction algorithm with CT-based physical corrections. Recently, Klein et al. demonstrated the feasibility and reproducibility of MBF measurement in a clinical setting using a dual-head SPECT/CT capable of rapid back-and-forth SPECT gantry rotation (Siemens Symbia; minimum SPECT frame duration = 10 s).[29] In a related study performed by Hsu et al., MFR and stress MBF measured using dynamic ^{99m}Tc-sestamibi SPECT/CT showed markedly enhanced CAD detection power as compared with conventional static SPECT, which provides semi-quantitative parameters, such as summed stress score and summed difference score[30] (Figure 5). However it should be noted that the extraction fraction of ^{99m}Tc myocardial perfusion imaging agents is far lower than that of PET tracers and the mitigation of the lower extraction fraction by means of K_1 uptake rate and MBF relationship amplify the random error of MBF measurement.

PET/CT AND PET/MRI

Design of current clinical PET and PET/CT scanners are primarily optimized for oncologic whole-body imaging studies (specifications of some commercially available PET/CT and PET/MR scanners for clinical use are summarized in Table 1). The axial length of PET detector rings ranges between 15 and 25 cm. This axial length is sufficient for scanning the human heart in a single bed position. The diameter of PET bore is about 70 cm to allow adequate space for obese patients and to avoid scan failure due to claustrophobia.

The main components of the PET detector are a scintillation crystal and a photosensor. The scintillation crystals primarily used in current clinical PET scanners are cerium-doped lutetium silicate scintillators (e.g., LSO, LGSO, and LYSO). These crystals have high stopping power for 511 keV gamma rays used in PET and fast decay time of scintillation light. The fast decay is critical in PET because the event rates in PET are much higher than those of SPECT using mechanical collimators. Fast PMTs are commonly used to measure the light photons generated in scintillation crystals. The analog and digital electronics employed to process output signals from photosensors and transfer data to storage devices have been enhanced. Collectively, the number of PET events that can be measured with manageable dead time have significantly increased.[39] This improvement in count rate performance enables the implementation of 3D dynamic myocardial PET studies without the use of interplane septa, thereby permitting absolute perfusion quantification.

The use of fast scintillation crystals and photosensors, in addition to the advances in electronics, enables measurement of the arrival time difference between two gamma ray photons (time-of-flight (TOF) information).[40,41] The accurate and precise TOF information enables the enhancement of PET image quality. Enhanced image quality for a given dosage is effective in reducing the noise level in PET time-activity curves, or the injection dosage of the subject.[42,43] An additional benefit of TOF information on myocardial PET studies is as follows: because TOF information competes with other physical artifacts in position determination, TOF PET is less sensitive to inconsistent correction data.[44,45] This is effective in reducing the artifacts attributed to the position mismatch between the emission PET image and attenuation map, which are commonly observed in myocardial PET studies. Furthermore, the performance of joint estimation (simultaneous reconstruction) algorithms of activity and attenuation employing only emission data can be enhanced by TOF information via intrinsic removal of mismatch artifacts. (Figure 6).[46]

PET spatial resolution has also been improved mainly because of the size reduction of scintillation crystals used in current systems. Increased resolving power of scintillation crystals in PET detector modules resulting from improved scintillation light generation and detection has enabled this crystal size reduction. Although the total number of crystals and the size of PET sinograms and reconstructed images have increased as a consequence of crystal size reduction, increased computer memory size, optimized data compression schemes, and advanced image reconstruction algorithms enable effective management and processing of large-sized data generated from 3D dynamic PET studies. Higher spatial resolution and image quality enhancement increases the sensitivity of PET for CAD detection.

Semiconductor Photosensor-based PET/MRI and PET/CT

A notable advancement in the field of PET instrumentation is the work on replacement of PMTs with semiconductor photosensors, such as the avalanche photodiode (APD) and silicon photomultiplier (SiPM). These semiconductor photosensors are relatively compact and impervious to magnetic fields, thus enabling simultaneous PET/MR image acquisition (Figure 7). The APD is more conventional, as it has about $\times\ 10^3$ electrical signal amplification gain, which is much higher than that of a regular photodiode but much smaller than that of the PMT (gain of approximately $\times\ 10^6$). APD-based PET detectors have primarily been used in PET and PET/MR systems customized for small animal use. Siemens Biograph mMR scanner (Siemens Healthcare GmbH, Erlangen, Germany) is the first commercial whole-body PET/MR scanner employing

Table 1. Specifications of some commercially available PET/CT and PET/MR scanners for clinical use

Vendor	General electric		Siemens		Philips		Toshiba
System	PET/CT	PET/MR	PET/CT	PET/MR	PET/CT	PET/MR	PET/CT
Product name	D-690	Signa	mCT	mMR	Vereos	Ingenuity	Celesteion
Photosensor	PMT	SiPM	PMT	APD	SiPM	PMT	PMT
Scintillation crystal	LYSO	Lu-based	LSO	LSO	LYSO	LYSO	LYSO
Crystal area (mm^2)	4.2 × 6.3	4.0 × 5.3	4 × 4	4 × 4	4 × 4	4 × 4	4 × 4
Crystal thickness (mm)	25	25	20	20	22	22	12
Maximum axial length (cm)	15.7	25	21.8	25.8	16.3	18	20
Timing resolution (ps)	544	390	527	2,930	345	525	450
Spatial resolution (mm)	4.7	4.3	4.4	4.3	4.0	4.7	5.1
Energy resolution (%)	12.4	10.5	11.5	14.5	11.1	12	13.7
Reference	31	32	33	34	35	36	37,38

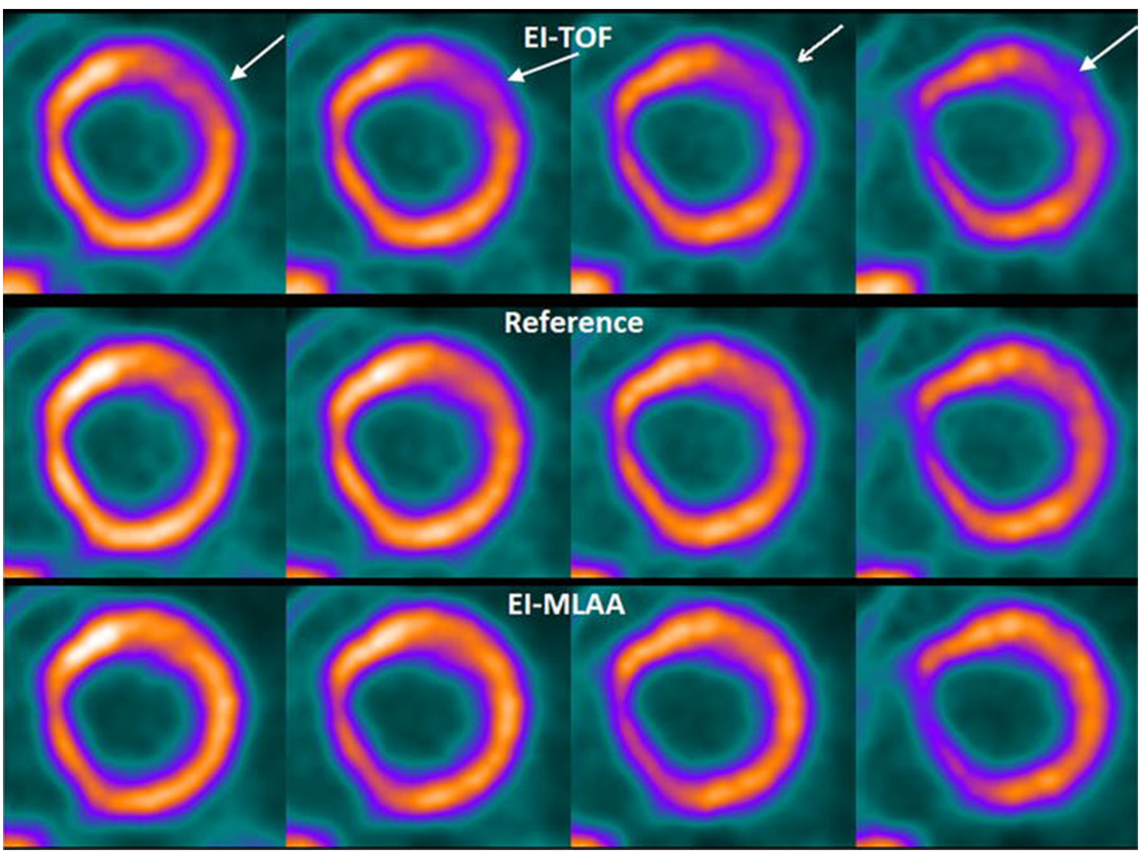

Figure 6. Removal of misalignment artifacts using a joint activity and attenuation estimation enhanced by TOF information. ^{13}N-ammonia PET images corrected for attenuation using (**A**) end-inspiration CT, **B** cine CT, and **C** joint estimation. (Reprint from Ref. Presotto et al.[46] with permission).

APD PET technology that allows simultaneous PET and MR image acquisition in the same field-of-view (FOV). In this scanner, eight rings of 56 PET detector modules were installed between the gradient and radiofrequency (RF) coils of 3T MRI.[34] PET system utilized in the mMR scanner yields higher geometric efficiency than that of the PET/CT systems from the same manufacturer (Biograph mCT). This is because mMR has a longer

PET axial FOV (25.8 cm) and smaller PET ring diameter (65.6 cm) than mCT (axial FOV: 21.8 cm, ring diameter: 84.2 cm). However, the gain of PET image quality thanks to the high geometric efficiency of mMR scanner is compromised by its poorer timing resolution (2.93 ns) of APD-based PET detectors relative to that of PMT-based detectors.

SiPM is another semiconductor photosensor that has led to significant advances in PET hardware technology in recent years. In the SiPM, micro avalanche photodiode (APD) cells operating in Geiger mode, i.e., the APD mode yielding its highest amplification gain, are connected in parallel. The SiPM has equivalent gain and rising time to the PMT, and higher photon detection efficiency than PMT; thus, SiPM-based PET detectors can yield better intrinsic performance than PMT and APD-based detectors. Several research groups have demonstrated the feasibility of SiPM PET and PET/MR imaging systems for small animal and brain imaging studies.[47–54] GE SIGNA PET/MR scanner (GE Healthcare, Waukesha, WI) is the first whole-body PET/MR scanner based on this new detector technology. The PET system in SIGNA PET/MR is comprised of five rings of 112 detector blocks, yielding an axial FOV of 25 cm and detector ring diameter of 60 cm (face-to-face: 62 cm).[32,55] The PET system features a timing resolution of < 400 ps, which is superior to the PMT-based PETCT scanner from the same manufacturer (544 ps, D-690).

SiPM technology has also been adopted in clinical PET/CT systems.[56] Philips Vereos (Philips Healthcare, Cleveland, OH) is the first commercial clinical PET/CT system that uses SiPM instead of PMT. The SiPM used in this scanner employs digital implementation of SiPM (Digital SiPM). In contrast to the analog SiPM, the

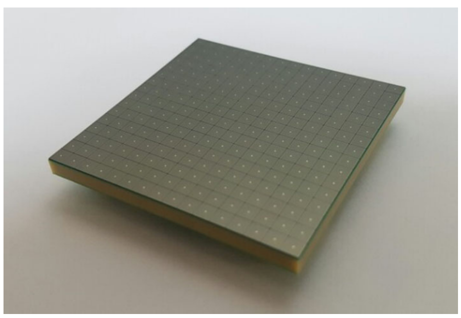

Figure 7. Silicon photomultiplier array (SiPM): an MRI-compatible solid-state photosensor.

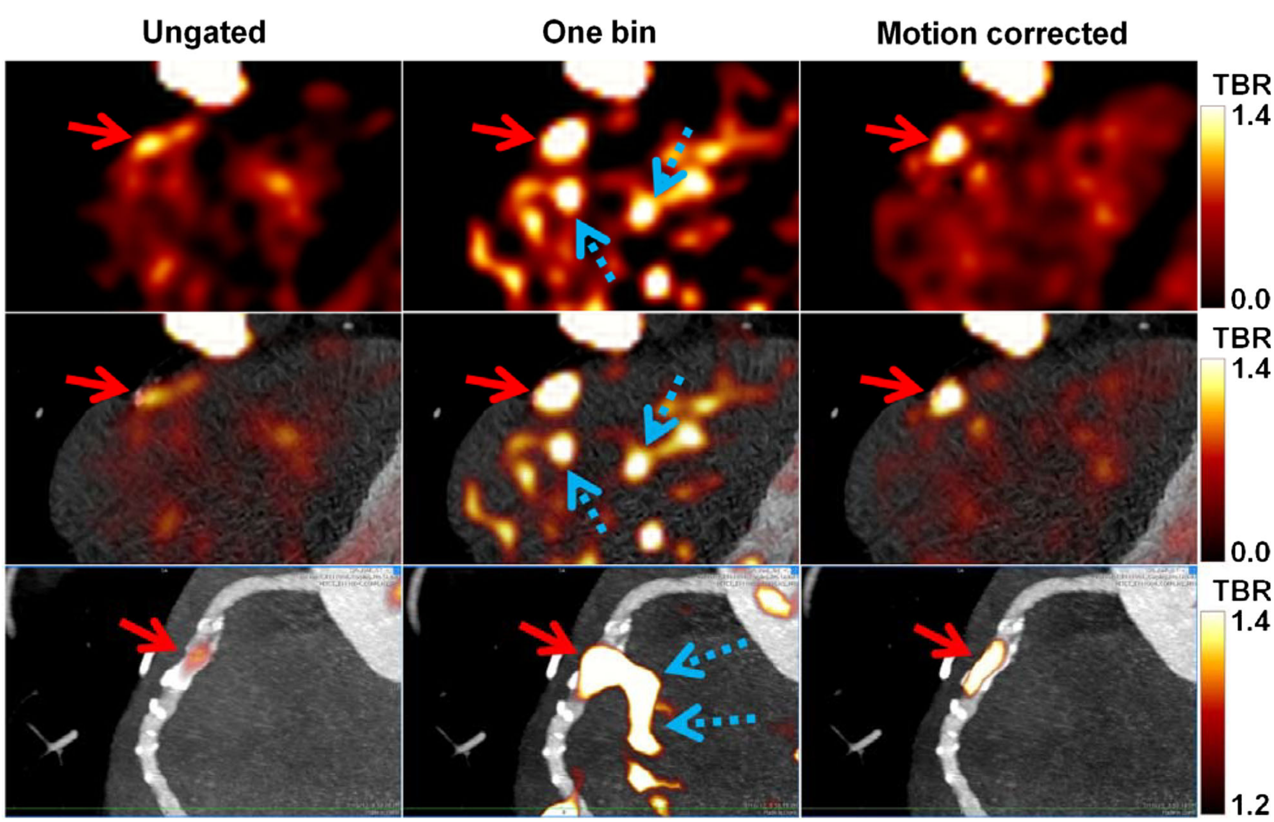

Figure 8. Non-linear motion correction of coronary plaque PET utilizing the extracted coronary arteries from CT angiography. (Reprint from Rubeaux et al.[69] with permission).

photosensor and data processing electronics are integrated onto a single silicon chip in the digital SiPM. Thus, the digital output of timing and energy information is provided in higher accuracy without necessitating off-chip time-to-digital and analog-to-digital convertors, which are the main sources of noise in conventional PET electronics. In addition, each digital SiPM is one-to-one coupled with an individual LYSO crystal element (4 × 4 × 19 mm) in the Vereos, leading to higher light collection efficiency. Due to these advanced features, substantial improvement in timing resolution (345 ps) is obtained in comparison with the current PMT-based PET/CT of Philips (Gemini TF: 495 ps; Ingenuity: 525 ps).[57,58]

Motion-Corrected Cardiac PET

In addition to the potential incorporation of ^{18}F-labled perfusion imaging agents,[59] advancements in the realm of PET spatial resolution and image quality are expected to further enhance PET performance for detection and quantification of regional myocardial ischemia.[6] Subendocardial perfusion measurements and quantification of the transmural perfusion gradient are promising applications where the enhanced PET performance will be valuable for increasing sensitivity and specificity of CAD detection.[60] Assessment of inflammation, angiogenesis, and microcalcification associated with atherosclerotic plaques in cardiac vessels is another beneficial result of enhanced PET performance.[61–65] However, such a benefit of high spatial resolution and improved image quality cannot be fully realized without proper cardiac and respiratory motion corrections.

Conventional gated PET images with multiple time bins have reduced image quality that is attributed to the limited number of PET counts. In contrast, the motion-corrected cardiac images of dual motion (cardiac and respiratory) correction schemes based on image registration techniques yield improvement of image resolution and contrast-to-noise ratio relative to those of ungated PET images.[66–68] Non-linear motion correction of coronary PET guided by the extracted coronary arteries from CT angiography is a particularly practical solution for problems reported in plaque imaging studies. Recently, Rubeaux et al. showed that this technique significantly reduced noise and increased target-to-background ratio in coronary ^{18}F-NaF PET images, thus increasing identification reliability of vulnerable plaque lesions[69] (Figure 8). Also noteworthy is the use of simultaneously acquired tagged MR images using an integrated PET/MR scanner for cardiac PET motion correction[70,71] (Figure 9). This method yields an estimation of motion and generation of motion-corrected PET images that is more robust and accurate than applying a PET-only approach.[71] An accelerated tagged MRI proposed recently would make this technique more compatible with routine clinical use.[70] The potential role of fat-MR-based coronary motion correction in improving coronary plaque PET images in simultaneous PET/MRI studies has also been demonstrated.[72]

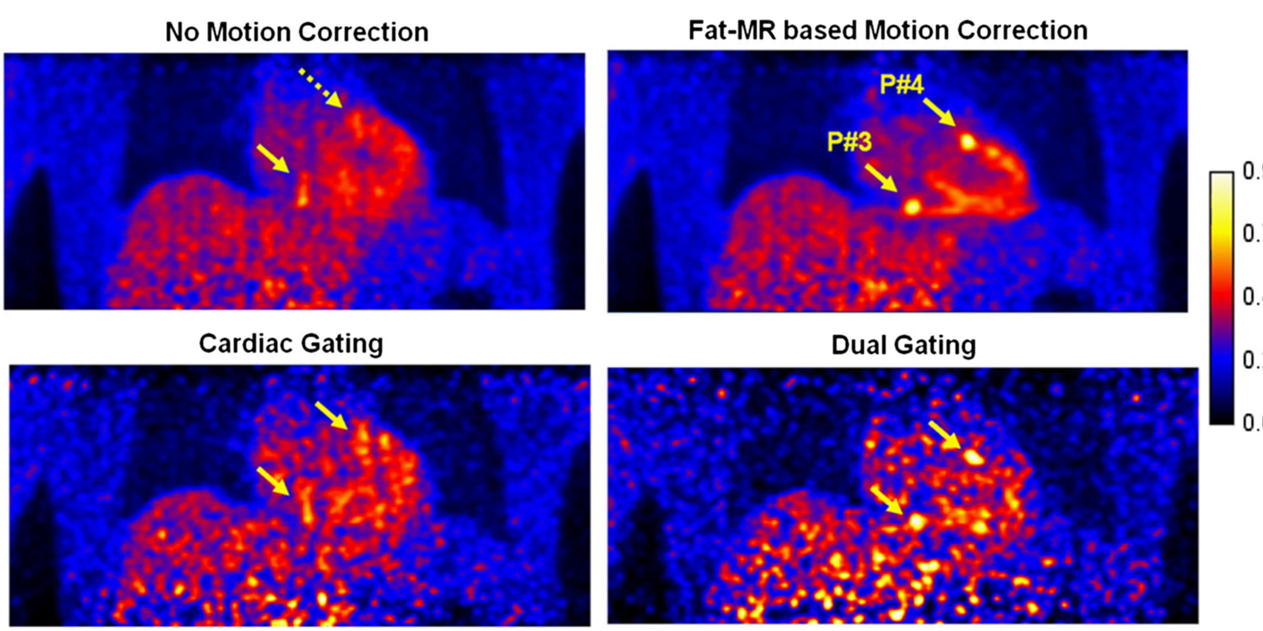

Figure 9. The effects of fat-MR-based coronary motion correction on plaque PET image quality as demonstrated by simulation. (Reprint from Petibon et al.[72] with permission).

CONCLUSIONS

Advances in iterative image reconstruction and CZT pixelated solid-state detectors have led to considerable system design and performance enhancements of dedicated cardiac SPECT scanners; these enhancements have subsequently reduced acquisition time and/or radiation dosage and enabled stationary fast dynamic SPECT scans. Absolute quantification of MBF and MFR based on kinetic analysis was a direct result of these enhancements. The improved hardware and software components of modern PET/CT and PET/MRI scanners, in addition to the recently developed cardiac PET imaging agents currently under study, are expected to further enhance PET performance in the assessment of various imaging biomarkers for cardiac diseases.[73] In particular, fully integrated PET/MRI systems utilizing advanced solid-state photosensors are suggested to provide new opportunities in nuclear cardiology.

NEW KNOWLEDGE GAINED

The present article reviews the current technology and recent developments in cardiac nuclear imaging, including SPECT, PET, PET-CT and new PET-MRI systems. Solid-state radiation detectors incorporating CZT are increasingly gaining favor as the detector of choice for application in dedicated cardiac SPECT systems. In addition, the improved quantitative SPECT/CT has the potential to measure the absolute quantification of myocardial blood flow and flow reserve. A notable advancement in the field of PET instrumentation is the work on replacement of PMTs with semiconductor photosensors, such as the APD and SiPM. Cardiac motion de-blurring aided by anatomical images is an emerging technique for further improvement of cardiac PET.

Acknowledgments

The authors would like to thank J-W Sohn for their assistance with manuscript preparation.

Disclosure

J.S. Lee, T. Sharir, and D.S. Lee have nothing to disclose. G. Kovalski is an employee of GE Healthcare.

References

1. Sharir T, Ben-Haim S, Merzon K, Prochorov V, Dickman D, Berman DS. High-speed myocardial perfusion imaging initial clinical comparison with conventional dual detector anger camera imaging. JACC Cardiovasc Imaging. 2008;1:156–63.
2. Esteves FP, Raggi P, Folks RD, Keidar Z, Askew JW, Rispler S, et al. Novel solid-state-detector dedicated cardiac camera for fast myocardial perfusion imaging: multicenter comparison with standard dual detector cameras. J Nucl Cardiol. 2009;16:927–34.
3. Sharir T, Slomka PJ, Hayes SW, DiCarli MF, Ziffer JA, Martin WH, et al. Multicenter trial of high-speed versus conventional single-photon emission computed tomography imaging: quantitative results of myocardial perfusion and left ventricular function. J Am Coll Cardiol. 2010;55:1965–74.
4. Chang SM, Nabi F, Xu J, Pratt CM, Mahmarian AC, Frias ME, et al. Value of CACS compared with ETT and myocardial perfusion imaging for predicting long-term cardiac outcome in asymptomatic and symptomatic patients at low risk for coronary disease: clinical implications in a multimodality imaging world. JACC Cardiovasc Imaging. 2015;8:134–44.
5. Rischpler C, Nekolla SG, Dregely I, Schwaiger M. Hybrid PET/MR imaging of the heart: potential, initial experiences, and future prospects. J Nucl Med. 2013;54:402–15.
6. Ratib O, Nkoulou R. Potential applications of PET/MR imaging in cardiology. J Nucl Med. 2014;55:40–5.
7. Nemallapudi MV, Gundacker S, Lecoq P, Auffray E, Ferri A, Gola A, et al. Sub-100 ps coincidence time resolution for positron emission tomography with LSO: Ce codoped with Ca. Phys Med Biol. 2015;60:4635–49.
8. Schug D, Wehner J, Dueppenbecker PM, Weissler B, Gebhardt P, Goldschmidt B, et al. PET performance and MRI compatibility evaluation of a digital, ToF-capable PET/MRI insert equipped with clinical scintillators. Phys Med Biol. 2015;60:7045–67.
9. Knoll P, Kotalova D, Köchle G, Kuzelka I, Minear G, Mirzaei S, et al. Comparison of advanced iterative reconstruction methods for SPECT/CT. Med Phys. 2012;22:58–69.
10. Borges-Neto S, Pagnanelli RA, Shaw LK, Honeycutt E, Shwartz SC, Adams GL, et al. Clinical results of a novel wide beam reconstruction method for shortening scan time of Tc-99m cardiac SPECT perfusion studies. J Nucl Cardiol. 2007;14:555–65.
11. Ali I, Ruddy TD, Almgrahi A, Anstett FG, Wells RG. Half-time SPECT myocardial perfusion imaging with attenuation correction. J Nucl Med. 2009;50:554–62.
12. Slomka PJ, Pan T, Berman DS, Germano G. Advances in SPECT and PET hardware. Prog Cardiovasc Dis. 2015;57:566–78.
13. Bocher M, Blevis IM, Tsukerman L, Shrem Y, Kovalski G, Volokh L. A fast cardiac gamma camera with dynamic SPECT capabilities: design, system validation and future potential. Eur J Nucl Med Mol Imaging. 2010;37:1887–902.
14. Imbert L, Poussier S, Franken PR, Songy B, Verger A, Morel O, et al. Compared performance of high-sensitivity cameras dedicated to myocardial perfusion SPECT: a comprehensive analysis of phantom and human images. J Nucl Med. 2012;53:1897–903.
15. Zoccarato O, Lizio D, Savi A, Indovina L, Scabbio C, Leva L, et al. Comparative analysis of cadmium-zincum-telluride cameras dedicated to myocardial perfusion SPECT: A phantom study. J Nucl Cardiol. 2016;23(4):885–93.
16. Duvall WL, Slomka PJ, Gerlach JR, Sweeny JM, Baber U, Croft LB, et al. High-efficiency SPECT MPI: comparison of automated quantification, visual interpretation, and coronary angiography. J Nucl Cardiol. 2013;20:763–73.
17. Einstein AJ, Blankstein R, Andrews H, Fish M, Padgett R, Hayes SW, et al. Comparison of image quality, myocardial perfusion, and left ventricular function between standard imaging and single-injection ultra-low-dose imaging using a high-efficiency SPECT camera: the MILLISIEVERT study. J Nucl Med. 2014;55:1430–7.
18. Sharir T, Pinskiy M, Pardes A, Rochman A, Prokhorov V, Kovalski G, et al. Comparison of the diagnostic accuracies of very low stress-dose with standard-dose myocardial perfusion imaging: Automated quantification of one-day, stress-first SPECT using a CZT camera. J Nucl Cardiol. 2016;23:11–20.

19. Ben-Haim S, Murthy VL, Breault C, Allie R, Sitek A, Roth N, et al. Quantification of myocardial perfusion reserve using dynamic SPECT imaging in humans: a feasibility study. J Nucl Med. 2013;54:873–9.
20. Ben Bouallègue F, Roubille F, Lattuca B, Cung TT, Macia JC, Gervasoni R, et al. SPECT myocardial perfusion reserve in patients with multivessel coronary disease: correlation with angiographic findings and invasive fractional flow reserve measurements. J Nucl Med. 2015;56:1712–7.
21. Shiraishi S, Sakamoto F, Tsuda N, Yoshida M, Tomiguchi S, Utsunomiya D, et al. Prediction of left main or 3-vessel disease using myocardial perfusion reserve on dynamic thallium-201 single-photon emission computed tomography with a semiconductor gamma camera. Circ J. 2015;79:623–31.
22. Mouden M, Ottervanger JP, Timmer JR, Reiffers S, Oostdijk AH, Knollema S, et al. The influence of coronary calcium score on the interpretation of myocardial perfusion imaging. J Nucl Cardiol. 2014;21:368–74.
23. Chang SM, Nabi F, Xu J, Peterson LE, Achari A, Pratt CM, et al. The coronary artery calcium score and stress myocardial perfusion imaging provide independent and complementary prediction of cardiac risk. J Am Coll Cardiol. 2009;54:1872–82.
24. Bailey DL, Willowson KP. An evidence-based review of quantitative SPECT imaging and potential clinical applications. J Nucl Med. 2013;54:83–9.
25. Slomka PJ, Berman DS, Germano G. Absolute myocardial blood flow quantification with SPECT/CT: is it possible? J Nucl Cardiol. 2014;21:1092–5.
26. Garcia EV. Are SPECT measurements of myocardial blood flow and flow reserve ready for clinical use? Eur J Nucl Med Mol Imaging. 2014;41:2291–3.
27. Wells RG, Timmins R, Klein R, Lockwood J, Marvin B, deKemp RA, et al. Dynamic SPECT measurement of absolute myocardial blood flow in a porcine model. J Nucl Med. 2014;55:1685–91.
28. Alhassen F, Nguyen N, Bains S, Gould RG, Seo Y, Bacharach SL, et al. Myocardial blood flow measurement with a conventional dual-head SPECT/CT with spatiotemporal iterative reconstructions - a clinical feasibility study. Am J Nucl Med Mol Imaging. 2013;4:53–9.
29. Klein R, Hung GU, Wu TC, Huang WS, Li D, deKemp RA, et al. Feasibility and operator variability of myocardial blood flow and reserve measurements with ^{99m}Tc-sestamibi quantitative dynamic SPECT/CT imaging. J Nucl Cardiol. 2014;21:1075–88.
30. Hsu B, Chen FC, Wu TC, Huang WS, Hou PN, Chen CC, et al. Quantitation of myocardial blood flow and myocardial flow reserve with ^{99m}Tc-sestamibi dynamic SPECT/CT to enhance detection of coronary artery disease. Eur J Nucl Med Mol Imaging. 2014;41:2294–306.
31. Bettinardi V, Presotto L, Rapisarda E, Picchio M, Gianolli L, Gilardi MC. Physical performance of the new hybrid PET/CT Discovery-690. Med Phys. 2011;38:5394–411.
32. Grant AM, Deller TW, Khalighi MM, Maramraju SH, Delso G, Levin CS. NEMA NU 2-2012 performance studies for the SiPM-based ToF-PET component of the GE SIGNA PET/MR system. Med Phys. 2016;43:2334.
33. Jakoby BW, Bercier Y, Conti M, Casey ME, Bendriem B, Townsend DW. Physical and clinical performance of the mCT time-of-flight PET/CT scanner. Phys Med Biol. 2011;56:2375–89.
34. Delso G, Fürst S, Jakoby B, Ladebeck R, Ganter C, Nekolla SG, et al. Performance measurements of the Siemens mMR integrated whole-body PET/MR scanner. J Nucl Med. 2011;52:1914–22.
35. Miller M, Zhang J, Binzel K, Griesmer J, Laurence T, Narayanan M, et al. Characterization of the Vereos digital photon counting PET system. J Nucl Med. 2015;56(suppl 4):434.
36. Zaidi H, Ojha N, Morich M, Griesmer J, Hu Z, Maniawski P, et al. Design and performance evaluation of a whole-body Ingenuity TF PET-MRI system. Phys Med Biol. 2011;56:3091–106.
37. Burr KC, Wang GCJ, Du H, Mann G, Balakrishnan K, Wang J, et al. A new modular and scalable detector for a time-of-flight PET scanner. Nuclear Science Symposium and Medical Imaging Conference (NSS/MIC). 2012; doi:10.1109/NSSMIC.2012.6551645.
38. Toshiba America Medical Systems Celesteion PET/CT Brochure. https://medical.toshiba.com/download/pop-up-ct-br-celesteion.
39. Moody JB, Lee BC, Corbett JR, Ficaro EP, Murthy VL. Precision and accuracy of clinical quantification of myocardial blood flow by dynamic PET: a technical perspective. J Nucl Cardiol. 2015;22:935–51.
40. Lee JS, Kim JH. Recent advances in hybrid molecular imaging systems. Semin Musculoskelet Radiol. 2014;18:103–22.
41. Ullah MN, Pratiwi E, Cheon J, Choi H, Yeom JY. Instrumentation for time-of-flight positron emission tomography. Nucl Med Mol Imaging. 2016;50:112–22.
42. Surti S, Karp JS. Advances in time-of-flight PET. Phys Med. 2016;32:12–22.
43. Vandenberghe S, Mikhaylova E, D'Hoe E, Mollet P, Karp JS. Recent developments in time-of-flight PET. EJNMMI Phys. 2016;3:3.
44. Conti M. Why is TOF PET reconstruction a more robust method in the presence of inconsistent data? Phys Med Biol. 2011;56:155–68.
45. Mehranian A, Zaidi H. Impact of time-of-flight PET on quantification errors in MR imaging-based attenuation correction. J Nucl Med. 2015;56:635–41.
46. Presotto L, Busnardo E, Perani D, Gianolli L, Gilardi MC, Bettinardi V. Simultaneous reconstruction of attenuation and activity in cardiac PET can remove CT misalignment artifacts. J Nucl Cardiol. 2016;23:1086–97.
47. Kwon SI, Lee JS, Yoon HS, Ito M, Ko GB, Choi JY, et al. Development of small-animal PET prototype using silicon photomultiplier (SiPM): initial results of phantom and animal imaging studies. J Nucl Med. 2011;52:572–9.
48. Yoon HS, Ko GB, Kwon SI, Lee CM, Ito M, Song IC, et al. Initial results of simultaneous PET/MRI experiments with an MRI-compatible silicon photomultiplier PET scanner. J Nucl Med. 2012;53:608–64.
49. Yamamoto S, Watabe T, Watabe H, Aoki M, Sugiyama E, Imaizumi M, et al. Simultaneous imaging using Si-PM-based PET and MRI for development of an integrated PET/MRI system. Phys Med Biol. 2012;57:N1–13.
50. Hong KJ, Choi Y, Jung JH, Kang J, Hu W, Lim HK, et al. A prototype MR insertable brain PET using tileable GAPD arrays. Med Phys. 2013;40:042503.
51. Olcott P, Kim E, Hong K, Lee BJ, Grant AM, Chang CM, et al. Prototype positron emission tomography insert with electro-optical signal transmission for simultaneous operation with MRI. Phys Med Biol. 2015;60:3459–78.
52. Wehner J, Weissler B, Dueppenbecker PM, Gebhardt P, Goldschmidt B, Schug D, et al. MR-compatibility assessment of the first preclinical PET-MRI insert equipped with digital silicon photomultipliers. Phys Med Biol. 2015;60:2231–55.
53. Ko GB, Yoon HS, Kim KY, Lee MS, Yang BY, Jeong JM, et al. Simultaneous multiparametric PET/MRI with silicon photomultiplier PET and ultra-high-field MRI for small-animal imaging. J Nucl Med. 2016;57:1309–15.
54. Jung JH, Choi Y, Im KC. PET/MRI: Technical challenges and recent advances. Nucl Med Mol Imaging. 2016;50:3–12.
55. Levin CS, Maramraju SH, Khalighi MM, Deller TW, Delso G, Jansen F. Design features and mutual compatibility studies of the

time-of-flight PET capable GE SIGNA PET/MR system. IEEE Trans Med Imaging. 2016;35:1907–14.

56. Miller MA, Jordan D, Laurence T, Laurence T, Muzic R, Narayanan M, et al. Initial characterization of a prototype digital photon counting PET system. J Nucl Med. 2014;55(suppl 1):658.
57. Nguyen NC, Vercher-Conejero JL, Sattar A, Miller MA, Maniawski PJ, Jordan DW, et al. Image quality and diagnostic performance of a digital pet prototype in patients with oncologic diseases: initial experience and comparison with analog PET. J Nucl Med. 2015;56:1378–85.
58. Boellaard R, Quick HH. Current image acquisition options in PET/MR. Semin Nucl Med. 2015;45:192–200.
59. Berman DS, Maddahi J, Tamarappoo BK, Czernin J, Taillefer R, Udelson JE, et al. Phase II safety and clinical comparison with single-photon emission computed tomography myocardial perfusion imaging for detection of coronary artery disease: flurpiridaz F 18 positron emission tomography. J Am Coll Cardiol. 2013;61:469–77.
60. Danad I, Raijmakers PG, Harms HJ, Heymans MW, van Royen N, Lubberink M, et al. Impact of anatomical and functional severity of coronary atherosclerotic plaques on the transmural perfusion gradient: a [^{15}O]H_2O PET study. Eur Heart J. 2014;35:2094–105.
61. Lee WW, Marinelli B, van der Laan AM, Sena BF, Gorbatov R, Leuschner F, et al. PET/MRI of inflammation in myocardial infarction. J Am Coll Cardiol. 2012;59:153–63.
62. Laitinen I, Saraste A, Weidl E, Poethko T, Weber AW, Nekolla SG, et al. Evaluation of alphavbeta3 integrin-targeted positron emission tomography tracer ^{18}F-galacto-RGD for imaging of vascular inflammation in atherosclerotic mice. Circ Cardiovasc Imaging. 2009;2:331–8.
63. Golestani R, Mirfeizi L, Zeebregts CJ, Westra J, de Haas HJ, Glaudemans AW, et al. Feasibility of [^{18}F]-RGD for ex vivo imaging of atherosclerosis in detection of $\alpha v\beta 3$ integrin expression. J Nucl Cardiol. 2015;22:1179–86.
64. Dweck MR, Chow MW, Joshi NV, Williams MC, Jones C, Fletcher AM, et al. Coronary arterial ^{18}F-sodium fluoride uptake: a novel marker of plaque biology. J Am Coll Cardiol. 2012;59:1539–48.
65. Shimizu Y, Kuge Y. Recent advances in the development of PET/SPECT probes for atherosclerosis imaging. Nucl Med Mol Imaging. 2016;50:284–91.
66. Kovalski G, Keidar Z, Frenkel A, Sachs J, Attia S, Azhari H. Dual, ''motion-frozen heart'' combining respiration and contraction compensation in clinical myocardial perfusion SPECT imaging. J Nucl Cardiol. 2009;16:396–404.
67. Lamare F, Le Maitre A, Dawood M, Schäfers KP, Fernandez P, Rimoldi OE, et al. Evaluation of respiratory and cardiac motion correction schemes in dual gated PET/CT cardiac imaging. Med Phys. 2014;41:072504.
68. Slomka PJ, Rubeaux M, Le Meunier L, Dey D, Lazewatsky JL, Pan T, et al. Dual-gated motion-frozen cardiac PET with flurpiridaz F 18. J Nucl Med. 2015;56:1876–81.
69. Rubeaux M, Joshi NV, Dweck MR, Fletcher A, Motwani M, Thomson LE, et al. Motion correction of ^{18}F-NaF PET for imaging coronary atherosclerotic plaques. J Nucl Med. 2016;57:54–9.
70. Huang C, Petibon Y, Ouyang J, Reese TG, Ahlman MA, Bluemke DA, et al. Accelerated acquisition of tagged MRI for cardiac motion correction in simultaneous PET-MR: phantom and patient studies. Med Phys. 2015;42:1087–97.
71. Chun SY, Reese TG, Ouyang J, Guerin B, Catana C, Zhu X, et al. MRI-based nonrigid motion correction in simultaneous PET/MRI. J Nucl Med. 2012;53:1284–91.
72. Petibon Y, El Fakhri G, Nezafat R, Johnson N, Brady T, Ouyang J. Towards coronary plaque imaging using simultaneous PET-MR: a simulation study. Phys Med Biol. 2014;59:1203–22.
73. Lee WW. Recent advances in nuclear cardiology. Nucl Med Mol Imaging. 2016;50:196–206.